CT Correlation With Outcomes in 15 Patients With Acute Middle East Respiratory Syndrome Coronavirus

Karuna M. Das[1]
Edward Y. Lee[2]
Mushira A. Enani[3]
Suhaila E. AlJawder[4]
Rajvir Singh[5]
Salman Bashir[6]
Nizar Al-Nakshbandi[1,7]
Khalid AlDossari[1]
Sven G. Larsson[1]

OBJECTIVE. The purpose of this article is to retrospectively analyze chest CT findings for 15 patients with Middle East respiratory syndrome coronavirus and to identify features associated with survival.

MATERIALS AND METHODS. Patients were assigned to group 1 if they died ($n = 9$) and to group 2 if they made a full recovery ($n = 6$). Two reviewers scored chest radiographs and CT examinations for segmental involvement, ground-glass opacities, consolidation, and interstitial thickening.

RESULTS. Eight patients had ground-glass opacity (53%), five had ground-glass and consolidation in combination (33%), five had pleural effusion (33%), and four patients had interlobular thickening (27%). Of 281 CT findings, 151 (54%) were peripheral, 68 (24%) were central, and 62 (22%) had a mixed location. The number of involved lung segments was higher in group 1. The lower lobe was more commonly involved (mean, 12.2 segments) than in the upper and middle lobes combined (mean, 6.3 segments). The mean number of lung segments involved was 12.3 segments in group 1 and 3.4 segments in group 2. The CT lung score (mean ± SD, 15.78 ± 7.9 vs 7.3 ± 5.7, $p = 0.003$), chest radiographic score (20.8 ± 1.7 vs 5.6 ± 5.4; $p = 0.001$), and mechanical ventilation duration (13.11 ± 8.3 vs 0.5 ± 1.2 days; $p = 0.002$) were higher in group 1. All nine group 1 patients and three of six group 2 patients had pleural effusion ($p = 0.52$).

CONCLUSION. CT of patients with Middle East respiratory syndrome coronavirus predominantly showed ground-glass opacities, with peripheral lower lobe preference. Pleural effusion and higher CT lung and chest radiographic scores correlate with poor prognosis and short-term mortality.

Keywords: CT, ground-glass opacities, lung changes, MERS-CoV, pleural effusion, prognosis

DOI:10.2214/AJR.14.13671

Received August 15, 2014; accepted after revision October 11, 2014.

[1]Department of Medical Imaging, King Fahad Medical City, Riyadh 11525, Kingdom of Saudi Arabia. Address correspondence to K. M. Das (daskmoy@gmail.com).

[2]Departments of Radiology and Medicine, Pulmonary Division, Boston Children's Hospital and Harvard Medical School, Boston, MA.

[3]Department of Medicine, Infectious Disease, King Fahad Medical City, Riyadh, Kingdom of Saudi Arabia.

[4]Department of Pulmonary and Sleep Medicine, King Fahad Medical City, Riyadh, Kingdom of Saudi Arabia.

[5]Department of Cardiology, Hamad Medical Corporation, Doha, Qatar.

[6]Department of Biostatistics and Research, King Fahad Medical City, Riyadh, Kingdom of Saudi Arabia.

[7]Department of Radiology, King Saud University Hospital, Riyadh, Kingdom of Saudi Arabia.

AJR 2015; 204:736–742

0361–803X/15/2044–736

A major outbreak of the Middle East respiratory syndrome coronavirus (MERS-CoV) has recently been reported by health authorities in Riyadh, Saudi Arabia [1]. Most patients with MERS-CoV present with fever (98%), fever with cough (83%), and shortness of breath (72%) [2, 3]. Radiographic manifestations range from unilateral ground-glass opacities (43%) to increased bronchovascular markings (17%) and diffuse reticulonodular pattern (4%), with very high mortality rates [3, 4]. Hitherto, detailed CT imaging features of MERS-CoV have been reported in only a small number of patients [5]. The purpose of this study was to retrospectively analyze the chest CT images of patients with MERS-CoV and to identify the features associated with poor prognosis and death.

Materials and Methods

Patients

Our retrospective cohort comprised 45 patients (age range, 12–80 years; mean [± SD] age, 44.2 ± 16.1 years; 11 male and 34 female patients) who received a positive diagnosis of MERS-CoV between April 7, 2014, and May 30, 2014. At the initial outbreak of the disease, most infected patients were referred to King Fahad Medical City, Riyadh, with subsequent identification being performed at another two centers in the region at a later date. The initial chest radiograph was normal in eight patients (17.8%) and abnormal in 37 patients (82.2%). Fifteen patients (33.3%) underwent chest CT and formed the study population (age range, 20–80 years; mean age, 48 ± 17.9 years; six men and nine women) (Table 1). Two (13%) of these 15 patients were health care workers who were secondarily infected after direct contact with a patient with active

TABLE 1: Demographic and Clinical Characteristics of 15 Patients With Middle East Respiratory Syndrome Coronavirus

Patient No.	Age (y)	Sex	Type of Chest Pattern	CT Lung Score	Radiographic Score at Peak	Absolute Lymphocytic Count (×10^9 cells/L)	Platelet Count (×10^9 cells/L)	Final Outcome
1	50	Female	2	8	12	38.3	208	Recovered
2	20	Female	4	20	24	30	327	Died
3	31	Male	4	2	22	11	280	Died
4	44	Male	4	20	22	8	240	Died
5	28	Male	4	20	18	21	82	Died
6	54	Female	2	16	6	23.9	234	Recovered
7	60	Female	4	4	22	51.6	81	Died
8	63	Female	2	2	4	36.3	209	Recovered
9	57	Female	4	18	20	10.8	128	Died
10	65	Female	4	24	20	7.5	302	Died
11	65	Male	3	12	20	7.8	158	Died
12	21	Female	2	12	0	23.9	298	Recovered
13	63	Male	2	4	12	4	157	Recovered
14	80	Male	4	22	20	8.8	150	Died
15	31	Female	2	2	0	24.2	240	Recovered

MERS-CoV infection. The diagnosis of MERS-CoV was established according to World Health Organization criteria, and a confirmed case was defined as a suspected case with a positive result for MERS-CoV on real-time polymerase chain reaction [4]. The permission for retrospective analysis of these patients with MERS-CoV infection was obtained from the institutional review board.

Imaging Technique

The Discovery CT750 HD scanner (120 kV and 140 mA; GE Healthcare) was used for all chest CT examinations. CT was performed with the patient in the supine position. IV contrast agent was used in patients with a high suspicion of pulmonary thromboembolism ($n = 5$). Because the study was a retrospective analysis, no standard protocol was applied. All patients were scanned with 64 × 0.625 mm collimation. In five patients with suspected pulmonary embolism, the helical 1.2-mm section thickness was reconstructed to 1 mm with a 1.25-mm interval for the transverse scans. In four patients, the helical 1.2-mm section thickness was reconstructed to 1 mm with a 6-mm interval for the transverse scans. In six patients, the helical 1.2-mm section thickness was reconstructed to 2.5 mm with a 2.5-mm interval for the transverse scans. Depending on the indications, the images were displayed with three different gray scales for interpretation of lung window, mediastinal window, and pulmonary embolism–specific settings. Sagittal and coronal scans with a 2.5-mm reformation were performed on all 15 patients.

The medical record of each patient was reviewed to obtain demographic characteristics and information on background diseases or conditions, symptoms, duration of hospitalization, admission to ICU, initiation and duration of mechanical ventilation, and death. All patients discharged from the hospital were contacted within a week by telephone and were asked to report any further symptoms, additional medical treatment, rehospitalization, and current status.

Image Interpretation

All chest CT examinations were reviewed independently by two radiologists with 8 and 20 years, respectively, of experience in interpreting chest CT. Interobserver variation was calculated. When there was a difference of opinion, a third radiologist with 30 years of experience in interpreting chest CT was consulted.

The CT examinations were reviewed on a dedicated radiology PACS (Centricity 2.1.2.1, GE Healthcare). The definitions of ground-glass opacities, consolidation, tree-in-bud, crazy paving, and septal thickening were the same as those described elsewhere [6]. Attention was paid to the presence of lung necrosis [7], cavitations, nodules, and interlobular and intralobular interstitial thickening. In addition, the presence of lymphadenopathy, pleural effusion, and pneumothorax was recorded. The CT findings in the outer third of the lung were defined as peripheral, and findings in the inner two thirds of the lung were defined as central. Each lung was divided into upper, middle, and lower zones [8], and each zone was reviewed for opacification. The size of the CT lesion was defined as described elsewhere [9]. The progression of MERS-CoV lesions within each lung zone was evaluated by scoring each zone from 0 (normal) to 4, with 4 corresponding to nearly total involvement of the lung parenchyma (Fig. 1). The scores were combined for all six zones to provide a total score ranging from 0 to 24, depending on the involvement of lung parenchyma [8].

The radiographs were reviewed separately from the CT scans and were evaluated for the development of areas of opacification. The series of frontal chest radiographs obtained during treatment were used to judge disease progression,

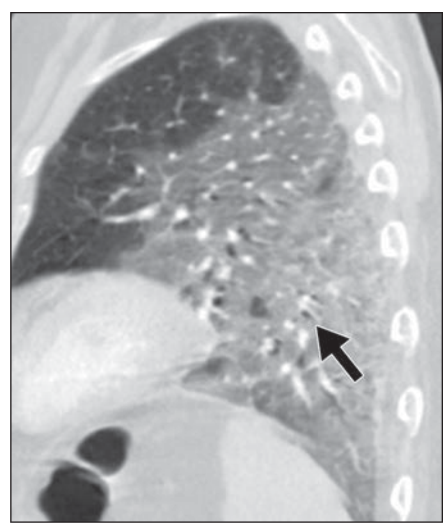

Fig. 1—57-year-old woman (patient 9) who presented with severe difficulty breathing and fever. Contrast-enhanced sagittal reformation CT performed on second day after admission shows ground-glass opacity (*arrow*) occupying almost three quarters of left hemithorax, equivalent to CT lung score of 8.

which was classified as described by Wong et al. [10], with minor modification of the definitions of types 2 and 3 disease progression. The definitions of type 1 (initial radiographic deterioration followed by improvement) and type 4 (progressive radiographic deterioration) disease progression (Fig. 2) were as described elsewhere [10]. Type 2 disease progression was defined as initial radiographic deterioration by one peak level, followed by radiographic improvement, with one peak level defined as overall mean lung parenchyma involvement more than 25% of the initial extent of involvement. Type 3 disease progression was defined as fluctuating radiographic changes, with at least two radiographic peaks and an intervening mild remission, which differed by more than 25% from overall mean lung involvement.

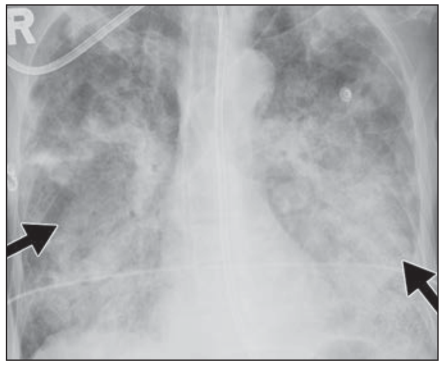

Fig. 2—28-year-old man (patient 5) who presented with severe cough and respiratory distress. Frontal chest radiograph shows type 4 disease progression with bilateral extensive airspace disease (*arrows*). Patient died on day 16 after symptom onset.

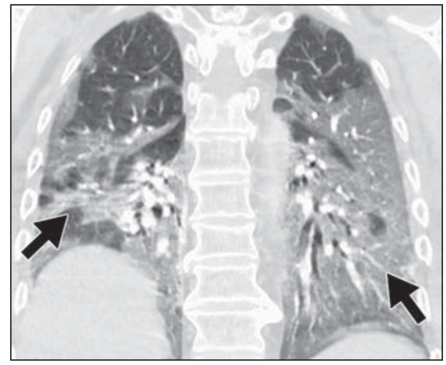

Fig. 3—57-year-old woman (patient 9; same patient as in Fig. 1) who presented with severe difficulty breathing and fever. Patient had multiple brain metastases with pulmonary embolism. Coronal CT reformation performed on second day of admission shows bilateral ground-glass type opacity on either side of chest (*arrows*). Patient died on day 18 after ICU admission after acute respiratory distress syndrome.

Statistical Analysis

The 15 patients were divided into two groups according to final outcome. Group 1 included nine patients with a final outcome of death, and group 2 included six patients with a final outcome of recovery. The CT lung score (range, 0–24), chest radiographic score, pattern of disease progression in chest radiographs (types 1–4), and presence or absence of other CT parameters (ground-glass opacification, consolidation, cavitation, pleural effusion, tree-in-bud, crazy paving, lung necrosis, intralobular thickening, and interlobular thickening) were compared between the two groups using a chi-square test for categoric data and Student *t* test for continuous variables. Demographic characteristics, comorbidity, platelet count, and absolute lymphocytic count were also compared between the two groups. Kaplan-Meier survival curve analysis was performed for the number of days the patient received mechanical ventilation. Interobserver variability was calculated using kappa statistics. Quantitative variables are presented as mean ± SD, and qualitative variables are presented as frequency and percentage. A p value (two-tailed) less than 0.05 was considered statistically significant. SPSS software (version 21.0, IBM) was used for statistical analysis.

Results

The 15 patients who underwent CT examination and who form the study sample initially presented with the following symptoms: difficulty breathing (n = 13), fever (n = 13), cough (n = 6), rhinitis (n = 2), diarrhea (n = 2), chest pain (n = 1), and sore throat (n = 1). The indications for CT included typical symptoms with normal chest radiograph in patients who had been in close contact with patients with active MERS-CoV infection (n = 2; 13%), continuous deterioration of clinical status and lack of response to treatment (n = 7), suspected pulmonary embolism (n = 5), and requirement for change of treatment with additional immunomodulation therapy (n = 1). In one patient, a follow-up CT scan was performed on day 8 of the ICU stay to evaluate the response to therapy. All 15 patients were monitored daily with frontal chest radiographs during the active phase of the disease. Twelve patients (80%) were admitted to the ICU because of respiratory failure, and all required mechanical ventilator support. Two patients (13.3%) were healthy hospital workers, and 13 patients had multiple comorbidities. Comorbidities were diabetes mellitus (n = 5), hypertension (n = 5), ischemic heart disease (n = 4), end-stage renal disease (n = 4), lymphoma (n = 2), asthma (n = 2), chronic obstructive pulmonary disease (n = 1), smoking (n = 1), intracranial metastases (n = 1), cardiac mass (n = 1), lung fibrosis (n = 1), postoperative status (n = 1), leukemia (n = 1), congestive heart failure (n = 1), pulmonary embolism (n = 1), acute myeloid leukemia (n = 1), and multiple myeloma (n = 1). The average number of comorbidities was 2.7 ± 1.13 for patients in group 1 and 1.3 ± 0.74 for patients in group 2 (p = 0.023). The total length of hospitalization was 15.2 ± 8 days (median, 15 days) in group 1 and 13.5 ± 10.7 days (median, 10.5 days) in group 2. Age was similar in the two groups (50 ± 20.2 vs 47 ± 17.3 years; p = 0.76).

CT was performed 5.22 ± 3.9 days after admission to the hospital. The details of the CT findings are summarized in Table 2. Ground-glass opacity (Fig. 3) was the earli-

TABLE 2: CT Findings for 15 Patients With Middle East Respiratory Syndrome Coronavirus

CT Findings	No. (%) of Patients	Days After Admission When CT Was Performed		
		2–5	6–9	10–13
Ground-glass opacity	13 (86.6)	8 (53)	1 (6.6)	4 (27)
Consolidation	5 (33.3)	3 (20)	0	2 (13)
Ground-glass opacity plus consolidation	9 (60)	5 (33)	2 (13)	2 (13)
Cavitation	1 (6.6)	0	0	1 (6.6)
Crazy paving	4 (27)	3 (20)	0	1 (6.6)
Tree in bud	1 (6.6)	1 (6.6)	0	0
Interlobular thickening	6 (40)	4 (27)	0	2 (13)
Intralobular thickening	3 (20)	2 (13)	0	1 (6.6)
Pulmonary fibrosis with emphysema	1 (6.6)	0	0	1 (6.6)
Pleural effusion	9 (60)	5 (33)[a]	0	4 (27)[a]

[a]These patients died.

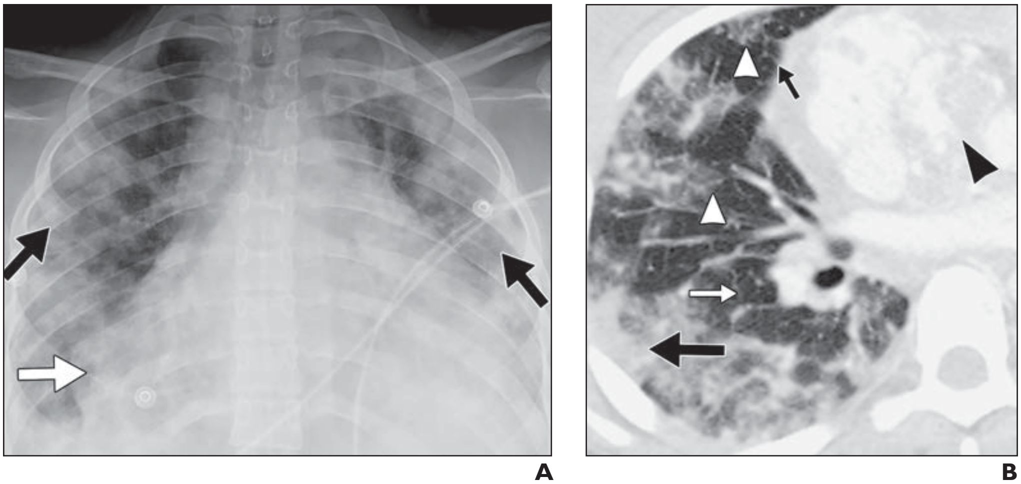

Fig. 4—20-year-old woman (patient 2) who presented with cough and difficulty breathing.
A, Frontal chest radiograph shows bilateral peripheral of ground-glass opacities (*black arrows*), along with enlarged heart due to right atrial cardiac mass (*white arrow*).
B, Contrast-enhanced transverse CT performed on third day of admission shows peripheral ground-glass opacities (*white arrowheads*) with consolidation (*thick black arrow*) and interlobular septal thickening (*thin black and white arrows*) and irregular right atrial mass (*black arrowhead*). Patient died in ICU after acute respiratory distress syndrome.

est CT finding (2–5 days) in eight patients (53%), followed by ground-glass and consolidation in combination ($n = 5$; 33%) (Fig. 4), pleural effusion ($n = 5$; 33%), and interlobular thickening ($n = 4$; 27%) (Fig. 5). Crazy paving with thicker interlobular and intralobular septa, cavitation (Fig. 6), tree-in-bud, and organizing pneumonia (Fig. 7) were observed in isolated cases. The average number of lung segments involved was 12.3 segments for group 1 (range, 6–16 segments; mean, 9.7 ± 3.5 segments) and 3.4 segments (range, 1–7 segments; mean, 2.6 ± 1.7 segments) for group 2. In group 1, the number of lung segments involved was higher in the lower lobe than in the upper and middle lobes combined (average of 12.2 segments for the lower lobe vs 6.3 segments for upper and middle lobes). Of the 281 lesions detected by CT, 151 (54%) were peripherally located (Fig. 8), 68 (24%) were centrally located, and 62 (22%) had a mixed location (Fig. 6). A higher proportion of CT findings (1 to < 3 cm) were seen in group 1 (34%) than in group 2 (29%) (Table 3). Reticulations were present in two of the nine patients with intralobular and interlobular septal thickening. Architectural distortion with traction type of bronchiectasis was present in the patient with a history of lung fibrosis (Fig. 9), and the identification of the CT features that were due to MERS-CoV was difficult, even with the third reviewer. Interobserver variability was good (κ = 0.70) for contrast-enhanced CT image findings.

The pattern of disease progression identified from chest radiographs (types 1–4) was significantly different across the two groups ($p = 0.001$). Nine subjects had type 4 disease progression, and radiographs showed progressive deterioration until the lungs became completely consolidated or the subject died. The time to peak for the progression of consolidation (Table 4) was 9.5 ± 3.3 days in group 1 and 5.8 ± 1.6 days in group 2 ($p = 0.019$). Pleural effusion was noted in all nine patients in group 1 and three of the six patients in group 2 ($p = 0.52$). Of the nine patients who died in the ICU, five had developed secondary infection isolated from the nasopharyngeal aspirate, as follows: *Pseudomonas* species ($n = 3$), methicillin-resistant *Staphylococcus aureus* ($n = 1$), and *Stenotrophomonas maltophilia* and *Pseudomonas* species ($n = 1$). Bronchosco-

TABLE 3: Lung Segments Involved, by Size and Position on CT

CT Findings	Group 1 ($n = 233$)	Group 2 ($n = 48$)	Total ($n = 281$)
CT lesion size			
< 1 cm	28 (12)	9 (19)	37 (13)
1 to < 3 cm	80 (34)	14 (29)	94 (33)
3 cm to < 50% of segment	57 (24)	21 (44)	78 (28)
50% of segment or more	68 (29)	4 (8)	72 (26)
Position on CT			
Central	62 (27)	6 (13)	68 (24)
Peripheral	120 (52)	31 (65)	151 (54)
Mixed	51 (22)	11 (23)	62 (22)

Note—Data are number (%) of lung segments.

TABLE 4: Comparison of Final Outcome According to Demographic and Clinical Characteristics

	Final Outcome		
Characteristics	Death ($n = 9$)	Recovered ($n = 6$)	p
Age (y)	50 ± 20.2	47 ± 17.3	0.764
No. of comorbidities per patient	2.7 ± 1.13	1.3 ± 0.74	0.023
Duration of mechanical ventilation (d)	13.11 ± 8.3	0.5 ± 1.2	0.002
CT lung score	15.78 ± 7.9	7.3 ± 5.7	0.003
Chest radiography score	20.8 ± 1.7	5.6 ± 5.4	0.001
Time to peak (d)	9.5 ± 3.3	5.8 ± 1.6	0.019
Absolute lymphocyte count (×10^9 cells/L)	17.3 ± 14.9	25.1 ± 12.2	0.295
Platelet count (×10^9 cells/L)	194.2 ± 94.7	224.3 ± 46.4	0.429

Note—Data are mean ± SD.

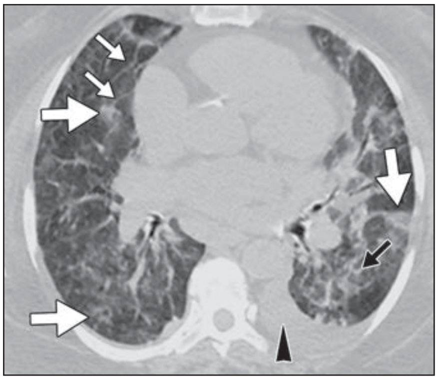

Fig. 5—65-year-old woman (patient 10) with end-stage renal disease who presented with difficulty breathing and fever. Transverse CT performed on 10th day of admission shows multiple ground-glass nodules (*thick white arrows*) with thickened interlobular (*thin white arrows*) and intralobular (*black arrow*) septum. Moderate pleural effusion was present (*arrowhead*). Patient died of acute respiratory distress syndrome in ICU after cholecystostomy.

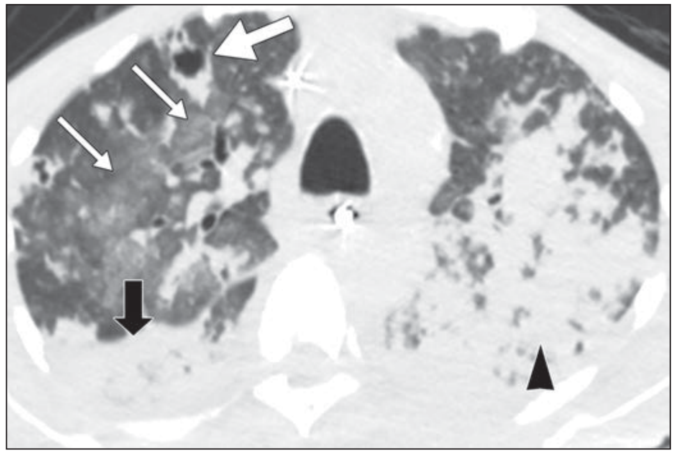

Fig. 6—44-year-old man (patient 4) with end-stage renal disease who presented with fever and cough with hemoptysis. Transverse CT performed on 10th day of admission shows central ground-glass opacity (*thin white arrows*) with peripheral (*black arrow*) and mixed (*arrowhead*) consolidation with well-defined cavity (*thick white arrow*) in periphery of ground-glass opacity. Patient died on day 19 after ICU admission after acute respiratory distress syndrome.

py and bronchial lavage was not performed for any of these patients. Kaplan-Meier analysis shows only 15% chance for survival up to 30 days (Fig. 10).

The mean ICU length of mechanical ventilation for group 1 was 13.11 ± 8.3 days. Nine of 15 patients died in the ICU (60%), and the time to death ranged from 4 to 31 days (mean, 13 ± 8.3 days; median, 13.0 days). One of these nine patients who died was a health care worker who died after acute respiratory distress syndrome (ARDS). The CT lung score ($p = 0.003$), chest radiographic score ($p = 0.001$), and duration of mechanical ventilation ($p = 0.002$) were higher in group 1 than in group 2 (Table 4). Of the six patients in group 2, one was rehospitalized with secondary infection of the lung, but this improved after treatment.

Discussion

MERS-CoV is a highly infectious disease and only preliminary data have been published on the causative agent. In this CT study, we showed ground-glass opacity to be the earliest CT finding, followed by ground-glass and consolidation in combination, pleural effusion, and interlobular thickening. There was a preference for involvement of the lower lobes, and most CT lesions were peripherally located. Our results suggest that peripheral subpleural focal ground-glass opacities and consolidations rapidly progressed to the rest of the lung and were responsible for ensuing ARDS in most patients (80%).

The higher CT lung and chest radiographic scores in group 1 compared with group 2 are related to the rapid progression of the disease process causing pneumonia that occupied maximum areas of lung in a relatively longer time to peak. The time to peak with complete recovery was shorter in group 2. Patients in group 2 were younger, had fewer comorbidities, had reduced lung segment involvement, had a lower prevalence of CT lung findings, and had a shorter mechanical ventilation duration in the ICU than did patients in group 1. These factors may have played a role in the recovery of patients in group 2.

The clinical, chest radiography, and CT features in our patients indicate the highly contagious nature and rapid progression of the disease. Wong et al. [10] reported that rapid progression of the disease with high chest radiographic score (type 4) was associated with high mortality in severe acute respiratory syndrome (SARS). Patients who died in our cohort had high CT scores (15.78 ± 7.9) and progressive radiographic scores (type 4) and showed deterioration despite medical treatment, indicating a virulent and fulminant course of the disease. Moreover, our cohort had a higher incidence of segmental involvement of the lung with rapid progression to ARDS than has been reported in patients with SARS [10]. Overall, mortality was 60% in our cohort. Similar to our experience, the mortality rate of MERS-CoV-infected patients has been reported to be approximately 60% [4, 11], compared with 9.6% in SARS [12]. The high rate of death in our cohort was further compounded by the high number of comorbidities, the longer time to peak, the longer duration of mechanical ventilation, and the presence of pleural effusion.

In the current study, the early appearance of pleural effusion in combination with higher CT lung and chest radiographic scores was a sign of poor prognosis and was associated with short-term mortality. Pleural effusion may play a significant role in the final outcome of patients with acute lung injury or ARDS in the ICU [13]. Although performance of a recruitment maneuver in the ICU can improve oxygenation in patients with ARDS, the improvement is hindered by the presence of pleural effusion [13]. This was similar in our cohort. In support of our findings, Hasley et al. [14] reported that the presence of bilateral pleural effusions was an independent predictor of short-term mortality

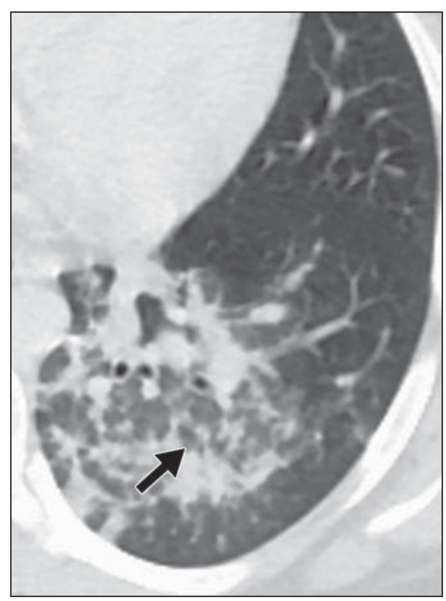

Fig. 7—21-year-old woman (patient 12) with acute myeloid leukemia who presented with fever and cough. Transverse contrast-enhanced CT performed on third day of admission shows organizing pneumonia in left lower lobe with perilobular pattern (*arrow*) occupying both central and peripheral location. Patient fully recovered after 4 days of mechanical ventilation in ICU.

Fig. 8—54-year-old woman (patient 6) who presented with fever, cough, and difficulty breathing. Transverse CT performed on 11th day of admission shows bilateral peripheral airspace consolidation (*arrows*). Patient fully recovered after 14 days of mechanical ventilation.

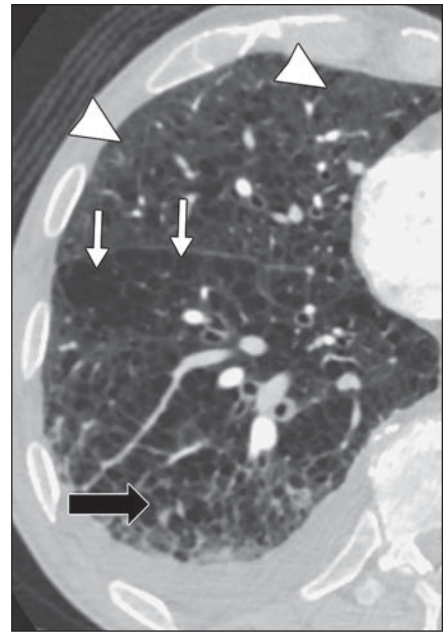

Fig. 9—80-year-old man (patient 14) with diabetes and lung fibrosis who presented with difficulty breathing and fever. Transverse contrast-enhanced CT performed on 10th day of admission shows multiple ill-defined areas of ground-glass type opacity (*arrowheads*) with intervening areas of lung fibrosis (*thick arrow*) and emphysema (*thin arrows*). No previous CT image was available for comparison. Patient died in ICU on day 12 after admission.

in patients with community-acquired pneumonia; however, in contrast to our experience, this relationship was absent in patients with SARS [9, 10].

The CT findings of tree-in-bud and lung cavitation were seen in isolated cases in our cohort but have not been reported in SARS or H1N1 influenza cases [9, 10, 15]. It is not possible to determine whether these CT findings were due to the MERS-CoV infection or some other secondary infection in the ICU; however, the patients with multicentric lung cavitation and tree-in-bud CT signs did not have any secondary infection, except for one patient with lung fibrosis and a methicillin-resistant *S. aureus* infection.

Peripheral airspace opacification was present in most of our cohort and was a hallmark of MERS-CoV. This has striking similarities with SARS [9, 10]. Like SARS, the CT and radiographic features of MERS-CoV may be indistinguishable from those of bacterial bronchopneumonia, organizing pneumonia, and acute interstitial pneumonia [16–18]. The presence of characteristic clinical features, close contact with an established MERS-CoV-infected patient, and early ground-glass appearance in chest radiographs or chest CT with lymphopenia should raise a high suspicion of MERS-CoV infection. Peripheral airspace opacities have also been noted in cases of atypical pneumonia caused by *Chlamydia* species, *Mycoplasma* species, *Legionella* species, H1N1 influenza, and other types of viruses that cause pneumonia in adults [15, 19–21]. The H1N1 influenza virus can cause homogeneous or patchy areas of ground-glass opacities, which consolidate with rapid progression to become confluent [15]. These areas of opacity may be unilateral or bilateral with rare occurrences of pleural effusion, which were more common in our cohort of patients with MERS-CoV. Hantavirus may cause similar viral pneumonia in immunocompetent adults and, patients present with a rapid onset of respiratory distress and rapidly progressing alveolar pulmonary edema, airspace consolidation, and pleural effusions [22]. A mortality rate of 46% has been reported with hantavirus infection, with a higher prevalence of pleural effusion [22]. By contrast, cytomegalovirus, herpesviruses, measles virus, and adenovirus mainly affect immunocompromised hosts [23–26]. These viral infections present with overlapping CT findings, such as poorly defined centrilobular nodules, ground-glass attenuation with a lobular distribution, segmental consolidation, and diffuse ground-glass attenuation with thickened interlobular septa [21].

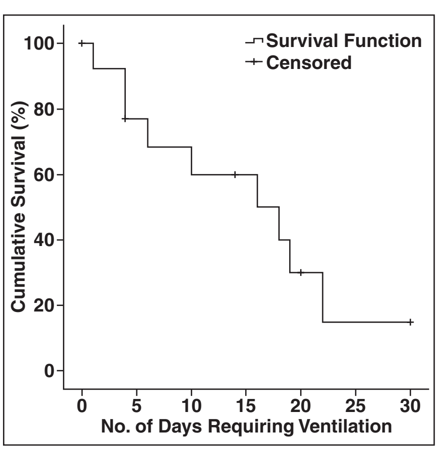

Fig. 10—Cumulative survival Kaplan-Meier curve showing ventilation days and probability of subjects' survival.

MERS-CoV is a new kind of viral infection, and the details of the pathologic process are yet to be understood. Like any other viral pneumonia, and as seen in two of our cases, the initial chest radiograph may be normal with subtle lung ground-glass opacities detected by CT [15]. MERS-CoV progresses rapidly within days in relationship to volume, extent, and severity [4]. In a previous study, the median time from symptom onset to hospitalization was 4.0 days and from symptom onset to death was 11.5 days [4]. The duration of hospitalization was short, with a median of 7.0 days and 9.0 days, respectively [4]. Similarly, in our cohort, time to death ranged from 4 to 31 days, with a median of 13.0 days, and the difference in median length of hospitalization between the groups was 15 and 10.5 days, respectively. The short incubation period with rapid progression to ARDS in more than 20% of patients with MERS-CoV (80% in our cohort) gives a very small window of opportunity for successful management of these high-risk patients [4]. Hence, an early diagnosis by CT in a highly suspicious clinical setting may help the initiation of effective treatment.

Low absolute lymphocytic count and low platelet count are two of the clinical indications of fatal outcome in patients with MERS-CoV [27]; however, we did not see a statistically significant difference between two groups in these variables. The high prevalence of lymphopenia in our patients may be related to cytokine dysregulation in patients with MERS-CoV, as postulated by an earlier group [28].

Health care workers are most likely to be in contact with severely infected individuals and are at high risk of infection. A highly infected patient with inherent comorbidities may be shedding viruses at a higher rate than mild or asymptomatic patients who are controlling the virus better [29]. Of two of the health care workers in our cohort, one died after contact with a high-risk primary patient with MERS-CoV. A high rate of underlying comorbidities in patients with MERS-CoV may create considerable difficulty in detecting the progress of the disease because of confounding from overlapping preexisting diseases such as lung fibrosis (Fig. 9) or emphysema.

We acknowledge two main limitations of our study. First, our cohort was small and sequential CT study was not performed because this was a retrospective analysis of a new disease; hence, we were not able to compare the early and late CT findings in patients with MERS-CoV. Moreover, for the same reason, we were only able to see the late sequelae of the disease in one patient, for whom complete recovery was noted. Future studies focusing on the disease progression should involve a large patient population. Second, we do not have histopathologic evidence of the inflammatory process for the patients who died in the course of the disease.

In summary, the CT features of patients with MERS-CoV were predominantly ground-glass opacities, with a preference for the involvement of the lower lobes in peripheral locations. The presence of pleural effusion and higher CT lung and chest radiographic scores indicate poor prognosis and short-term mortality.

References

1. Zaki AM, van Boheemen S, Bestebroer TM, Osterhaus AD, Fouchier RA. Isolation of a novel coronavirus from a man with pneumonia in Saudi Arabia. *N Engl J Med* 2012; 367:1814–1820
2. Hui DS, Memish ZA, Zumla A. Severe acute respiratory syndrome vs. the Middle East respiratory syndrome. *Curr Opin Pulm Med* 2014; 20:233–241
3. Al-Tawfiq JA, Assiri A, Memish ZA. Middle East respiratory syndrome novel corona MERS-CoV infection: epidemiology and outcome update. *Saudi Med J* 2013; 34:991–994
4. The WHO MERS-CoV Research Group. State of knowledge and data gaps of Middle East Respiratory Syndrome coronavirus (MERS-CoV) in humans. *PLoS Curr* 2013; 5:pii
5. Ajlan AM, Ahyad RA, Jamjoom LG, Alharthy A, Madani TA. Middle East respiratory syndrome coronavirus (MERS-CoV) infection: chest CT findings. *AJR* 2014; 203:782–787
6. Hansell DM, Bankier AA, MacMahon H, McLoud TC, Muller NL, Remy J. Fleischner Society: glossary of terms for thoracic imaging. *Radiology* 2008; 246:697–722
7. Sawicki GS, Lu FL, Valim C, Cleveland RH, Colin AA. Necrotising pneumonia is an increasingly detected complication of pneumonia in children. *Eur Respir J* 2008; 31:1285–1291
8. Ooi GC, Khong PL, Müller NL, et al. Severe acute respiratory syndrome: temporal lung changes at thin-section CT in 30 patients. *Radiology* 2004; 230:836–844
9. Wong KT, Antonio GE, Hui DS, et al. Thin-section CT of severe acute respiratory syndrome: evaluation of 73 patients exposed to or with the disease. *Radiology* 2003; 228:395–400
10. Wong KT, Antonio GE, Hui DS, et al. Severe acute respiratory syndrome: radiographic appearances and pattern of progression in 138 patients. *Radiology* 2003; 228:401–406
11. Assiri A, Al-Tawfiq JA, AlRabeeah AA, et al. Epidemiological, demographic, and clinical characteristics of 47 cases of Middle East respiratory syndrome coronavirus disease from Saudi Arabia: a descriptive study. *Lancet Infect Dis* 2013; 13:752–761
12. World Health Organization. Summary of probable SARS cases with onset of illness from 1 November 2002 to 31 July 2003. World Health Organization website. www.who.int/csr/sars/country/table2004_04_21/en/. Published December 31, 2003. Accessed October 31, 2008
13. Lan CC, Hsu HH, Wu CP, Lee SC, Peng CK, Chang H. Influences of pleural effusion on respiratory mechanics, gas exchange, hemodynamics, and recruitment effects in acute respiratory distress syndrome. *J Surg Res* 2014; 186:346–353
14. Hasley PB, Albaum MN, Li YH, et al. Do pulmonary radiographic findings at presentation predict mortality in patients with community-acquired pneumonia? *Arch Intern Med* 1996; 156:2206–2212
15. Agarwal PP, Cinti S, Kazerooni EA. Chest radiographic and CT findings in novel swine-origin influenza A (H1N1) virus (S-OIV) infection. *AJR* 2009; 193:1488–1493
16. Müller NL, Staples CA, Miller RR. Bronchiolitis obliterans organizing pneumonia: CT features in 14 patients. *AJR* 1990; 154:983–987
17. Lee KS, Kullnig P, Hartman TE, Muller NL. Cryptogenic organizing pneumonia: CT findings in 43 patients. *AJR* 1994; 162:543–546
18. Primack SL, Hartman TE, Ikezoe J, Akira M, Sakatani M, Muller NL. Acute interstitial pneumonia: radiographic and CT findings in nine patients. *Radiology* 1993; 188:817–820
19. Goodman LR, Goren RA, Teptick SK. The radiographic evaluation of pulmonary infection. *Med Clin North Am* 1980; 64:553–574
20. Macfarlane JT, Miller AC, Roderick Smith WH, Morris AH, Rose DH. Comparative radiographic features of community acquired Legionnaires disease, pneumococcal pneumonia, mycoplasma pneumonia and psittacosis. *Thorax* 1984; 39:28–33
21. Kim EA, Lee KS, Primack SL, et al. Viral pneumonias in adults: radiologic and pathologic findings. *RadioGraphics* 2002; 22: S137– S149
22. Boroja M, Barrie JR, Raymond GS. Radiographic findings in 20 patients with Hantavirus pulmonary syndrome correlated with clinical outcome. *AJR* 2002; 178:159–163
23. Kang EY, Patz EF, Müller NL. Cytomegalovirus pneumonia in transplant patients: CT findings. *J Comput Assist Tomogr* 1996; 20:295–299
24. Ramsey PG, Fife KH, Hackman RC, Meyers JD, Corey L. Herpes simplex virus pneumonia: clinical, virologic, and pathologic features in 20 patients. *Ann Intern Med* 1982; 97:813–820
25. Tanaka H, Honma S, Yamagishi M, et al. Clinical features of measles pneumonia in adults: usefulness of computed tomography. *Nihon Kyobu Shikkan Gakkai Zasshi* 1993; 31:1129–1133
26. Kawai T, Fujiwara T, Aoyama Y, et al. Diffuse interstitial fibrosing pneumonitis and adenovirus infection. *Chest* 1976; 69:692–694
27. Arabi YM, Arifi AA, Balkhy HH, et al. Clinical course and outcomes of critically ill patients with Middle East respiratory syndrome coronavirus infection. *Ann Intern Med* 2014; 160:389–397
28. Drosten C, Seilmaier M, Corman VM, et al. Clinical features and virological analysis of a case of Middle East respiratory syndrome coronavirus infection. *Lancet Infect Dis* 2013; 13:745–751
29. Zumla A, Hui SD. Infection control and MERS-Cov in health-care workers. *Lancet* 2014; 383:1869–1871